A Novel Target Detection and Identifying Approach Using Polarimetric Radar Cross-Section and Matrix Correlation Coefficient

Narathep Phruksahiran[†], Non-member

ABSTRACT

This paper presents a novel target detection and identifying approach using polarimetric radar cross-section and matrix correlation coefficient. We have adopted a polarimetric radar cross-section matrix correlation strategy (PRMC) algorithm using a matrix correlation approach based on the polarimetric radar cross-section. It is projected as an inverse scattering problem under the electromagnetic scattering model using polarimetric Physical Optics approximation. The experimental measurements using canonical targets carried out under semi controlled conditions verify the performance of the developed procedures. Finally, the identification strategies' effectiveness is demonstrated in free-space conditions and a scene with a brick and autoclaved aerated concrete wall.

Keywords: Polarimetric Radar Cross-Section, Matrix Correlation Coefficient, Physical Optics Approximation

1. INTRODUCTION

Through the Wall Radar Imaging (TWRI) has earned widespread attention in recent years. The TWRI technique can detect objects behind obstructions based on transmitting and receiving electromagnetic waves, encouraging it to be applied in various applications, such as rescue, surveillance, and observation procedures. However, the applicability of physical-based methods accurately provides the adaptable modelling of electromagnetic scattering from the canonical targets, [1].

1.1 Related Work

Numerous techniques are developed and used in TWRI procedures [2], such as the invention of electromagnetic wave propagation modeling, as shown by [3]-[4], the reducing methodology of the wall reflection effect, as presented by [5]-[6], the inverse scattering approach, as demonstrated in [7]-[8], and multiarray observation, as shown by [9]-[11], including the application based on amplitude-only using synthetic aperture radar configuration, as presented by [12]-[13]. Depending on the experimental design and implementation, the individual approach has diverse strengths and weaknesses.

From various techniques mentioned above, it can be considered that physical properties, including the amplitude of the scattered electromagnetic wave, are an essential characteristic that can be used to develop measurement and processing strategies to detect canonical objects behind an obstruction.

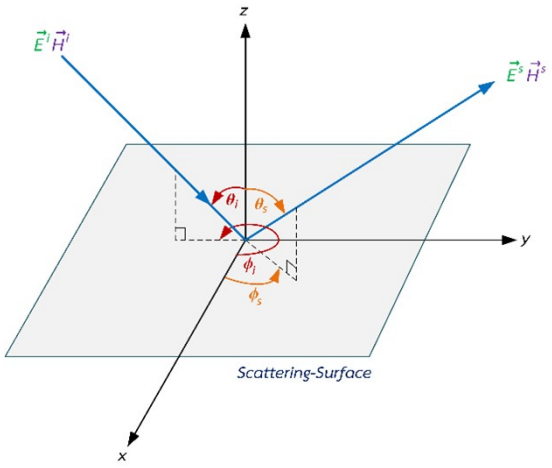

***Fig. 1**: Local coordinate system for PO calculation.*

1.2 Motivation and Contributions

Most research focuses on analysing the presence of objects behind walls or obstacles. In this research, we have considered the reflection properties of electromagnetic waves, which vary with the direction of incidence and polarisation of the waves. This paper presents a new polarimetric radar cross-section and matrix correlation strategy (PRMC) to detect and identify the canonical target shape through the wall without known target parameters. The novelty and advantage contributions of our work are listed as follows:

1) We combined polarimetric radar cross-section of canonical targets based on the Physical Optic approximation (PO) simulation and the actual received power measurement in bistatic radar configuration.

Manuscript received on April 24, 2023; revised on April 9, 2024; accepted on April 18, 2024. This paper was recommended by Associate Editor Siraporn Sakphrom.

The author is with Chulachomklao Royal Military Academy, Nakhon Nayok, Thailand,

[†]Corresponding author: narathepp@gmail.com

Digital Object Identifier: 10.37936/ecti-eec.2024222.249272

2) According to the proposed strategy, we designed the experiment set to be consistent with the simulation of electromagnetic wave reflection using developed mathematical models.

3) We have organized the reflection values into a matrix format with different polarizations, which can represent reflecting properties that vary according to the position and direction of the electromagnetic wave.

This paper is organized as follows. First, Section 2 presents the proposed system model and problem formulation approach. Then, Section 3 describes the experimental setup and the test cases considered. Next, Section 4 provides the simulation and experimental results using the proposed method. Finally, Section 5 contains the conclusions.

2. PROBLEM FORMULATION AND PRMC APPROACH

2.1 Scattering Mechanism

Electromagnetic wave propagation can be described using mathematical equations. According to [14], the scattering mechanism in the far-field can be represented as a transformation between incident electric fields $\overrightarrow{E^i}$ and scattered electric fields $\overrightarrow{E^s}$ as

$$\overrightarrow{E^s} = \frac{e^{-jkR}}{R} \left[\overrightarrow{S_{pq}}\right] \overrightarrow{E^i} \tag{1}$$

or

$$\overrightarrow{E^s} = \begin{bmatrix} E_h^s \\ E_v^s \end{bmatrix} = \frac{e^{-jkR}}{R} \begin{bmatrix} S_{hh} & S_{hv} \\ S_{vh} & S_{vv} \end{bmatrix} \begin{bmatrix} E_h^i \\ E_v^i \end{bmatrix}, \tag{2}$$

where S_{pq} are the complex scattering amplitude component of the scattering matrix $\left[\overrightarrow{S_{pq}}\right]$, in which the index p and q stand for the incident and scattered polarization, respectively. The index h and v denote the horizontal and vertical polarization basis of the wave.

The PO technique can be used to simulate the electric field intensity caused by the reflection of a canonical target's surface. According to [15]-[17], the relationship between the current distribution on the scattering surface $\overrightarrow{J_s}$, the incident magnetic field $\overrightarrow{H^i}$, and the unit vector perpendicular to the scatter surface $\hat{n}$ is

$$\overrightarrow{J_s} = 2\hat{n} \times \overrightarrow{H^i}, \tag{3}$$

including the electromagnetic field's orientation used in polarimetric radar cross-section simulation based on PO approximation. The incident angle is perpendicular to the target's surface from this geometry. However, the scattered angle will change depending on the position of the receiver antenna. The connection between magnetic and electric fields in electromagnetic wave propagation makes it practicable to estimate the value of $\overrightarrow{J_s}$ on the object surface by characterizing the incident electric field vector.

The scattered field in the far field region can be estimated by using the magnetic flux density $\overrightarrow{B}$, the vector potential $\overrightarrow{A}$,with $\overrightarrow{B} = \nabla \times \overrightarrow{A}$. By employing the characterization of vector notation with $\vec{r} = (x\hat{x} + y\hat{y} + z\hat{z})$ for observation point, $\overrightarrow{r'} = \left(x'^{\hat{x}} + y'^{\hat{y}} + z'^{\hat{z}}\right)$ for source point, ψ as the angel between vector $\vec{r}$ and $\overrightarrow{r'}$ and the approximation $R = r - r'^{\cos\psi}$, we get:

$$\begin{aligned} \overrightarrow{A}(x,y,z) &= \frac{\mu}{4\pi} \iint \overrightarrow{J_s}\left(x',y',z'\right) \frac{e^{-jkR}}{R}\, ds' \\ &\approx \frac{\mu e^{-jkr}}{4\pi r}\, \overrightarrow{N} \end{aligned} \tag{4}$$

with

$$\overrightarrow{N} = \iint \overrightarrow{J_s}\left(x',y',z'\right)\, e^{jkr'\cos\psi}\, ds' \tag{5}$$

The scattered electric field $\overrightarrow{\boldsymbol{E}^{\boldsymbol{s}}}$ in the far field region can be estimated by using the vector-potential $\overrightarrow{\boldsymbol{A}}$ and the angular frequency $\boldsymbol{\omega}$, as shown by [18] as:

$$\overrightarrow{E^s} = -j\omega\overrightarrow{A} \tag{6}$$

To a good approximation in the spherical coordinate system $\hat{\boldsymbol{r}}, \hat{\boldsymbol{\theta}}, \hat{\boldsymbol{\phi}}$, the components of the scattered electric field can be assumed as follows:

$$E_r^s \approx 0 \tag{7}$$

$$E_\theta^s \approx -\frac{jke^{-jkr}}{4\pi r}\, \eta N_\theta \tag{8}$$

$$E_\phi^s \approx -\frac{jke^{-jkr}}{4\pi r}\, \eta N_\phi \tag{9}$$

,where $\boldsymbol{\eta}$ is the impedance of free space. By using the coordinate transformation, the parameters $\boldsymbol{N_\theta}$ and $\boldsymbol{N_\phi}$ in the spherical coordinate system can be described from the parameters $\boldsymbol{J_x}$, $\boldsymbol{J_y}$ and $\boldsymbol{J_z}$ in the Cartesian coordinate system as:

$$\begin{aligned} N_\theta = \iint (&J_x\cos\theta_s\cos\phi_s + J_y\cos\theta_s\sin\phi_s \\ &- J_z\sin\theta_s)\, e^{jkr'\cos\psi}\, ds' \end{aligned} \tag{10}$$

$$N_\phi = \iint (-J_x\sin\phi_s + J_y\cos\phi_s) \bullet e^{jkr'\cos\psi}\, ds' \tag{11}$$

,where the angle identification $\boldsymbol{\theta_i}$, $\boldsymbol{\theta_s}$, $\boldsymbol{\phi_i}$ and $\boldsymbol{\phi_s}$ are illustrated in Fig. 1, by using the Cartesian coordinate system $\hat{\boldsymbol{x}}$, $\hat{\boldsymbol{y}}$ and $\hat{\boldsymbol{z}}$ axis on the scattering surface.

2.2 Polarimetric Radar Cross-Section

The direction of wave propagation and the orientation of the electric field directly influence the reflection of that electromagnetic wave back to the receiving antenna. The authors in [19] and [20] present the concepts and equations which can be used to simulate the polarized radar cross-section denoted $\boldsymbol{\sigma_{pq}}$ as:

$$\sigma_{pq} = \lim_{R\to\infty} 4\pi R^2 \frac{\left|\overrightarrow{E}_q^s\left(\theta_s,\ \phi_s\right)\right|^2}{\left|\overrightarrow{E}_p^i\left(\theta_i,\ \phi_i\right)\right|^2} \tag{12}$$

Based on the transformation of the electric field components from the spherical coordinate system denoted $(\boldsymbol{E_r}, \boldsymbol{E_\theta}, \boldsymbol{E_\phi})$ into the electrical field component in the Cartesian coordinate system indicated $(\boldsymbol{E_x}, \boldsymbol{E_y}, \boldsymbol{E_z})$ as:

$$E_x^s = E_r^s \sin\theta_s \cos\phi_s + E_\theta^s \cos\theta_s \cos\phi_s - E_\phi^s \sin\phi_s \tag{13}$$

$$E_y^s = E_r^s \sin\theta_s \sin\phi_s + E_\theta^s \sin\phi_s + E_\phi^s \cos\phi_s \tag{14}$$

$$E_z^s = E_r^s \cos\theta_s - E_\theta^s \sin\theta_s \tag{15}$$

By employing a horn antenna, the electromagnetic relations in horizontal and vertical polarization could be estimated and simulated, as depicted in Fig. 2. We consider that the $\boldsymbol{x}$ component and the $\boldsymbol{y}$ component of the scattered electric fields can be used for the horizontal and the vertical received mode, respectively, so that we can specify the polarized radar cross section as follows:

$$\sigma_{hh} = 4\pi r^2 \frac{\left|\overrightarrow{E}_h^s\left(\theta_s,\ \phi_s\right)\right|^2}{\left|\overrightarrow{E}_h^i\left(\theta_i,\ \phi_i\right)\right|^2} = 4\pi r^2 \frac{\left|\overrightarrow{E}_x^s\left(\theta_s,\ \phi_s\right)\right|^2}{\left|\overrightarrow{E}_h^i\left(\theta_i,\ \phi_i\right)\right|^2} \tag{16}$$

$$\sigma_{vv} = 4\pi r^2 \frac{\left|\overrightarrow{E}_v^s\left(\theta_s,\ \phi_s\right)\right|^2}{\left|\overrightarrow{E}_v^i\left(\theta_i,\ \phi_i\right)\right|^2} = 4\pi r^2 \frac{\left|\overrightarrow{E}_y^s\left(\theta_s,\ \phi_s\right)\right|^2}{\left|\overrightarrow{E}_h^i\left(\theta_i,\ \phi_i\right)\right|^2} \tag{17}$$

2.3 The Proposed PRMC Method

The central concept is to experiment with a mathematical model built from an electrical and magnetically field component model compared to the value obtained from the actual measurement. The model's accuracy is based on the correlation of the datasets arranged as a matrix. It corresponds to the physical model and computation of the received power, as described by [21], we can write the ratio of received power P_r to transmitted power P_t in the form of a radar range equation based on measurement as.

$$\frac{P_{r,pq}}{P_{t,pq}} = \sigma_{pq} \bullet \frac{G_{t,pq} G_{r,pq} \lambda^2}{(4\pi)^3 r_1^2 r_2^2} \tag{18}$$

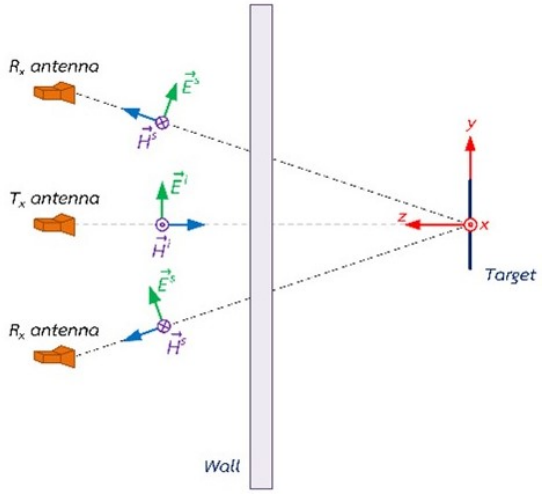

***Fig. 2**: Electric and magnetic fields components.*

or

$$\sigma_{pq} = \frac{P_{r,pq}}{P_{t,pq}} \bullet \frac{(4\pi)^3 r_1^2 r_2^2}{G_{t,pq} G_{r,pq} \lambda^2} \tag{19}$$

,where G_t is the gain of transmitting antenna, G_r is the gain of receiving antenna, λ is the wavelength, r_1 and r_2 are the distance along the propagation path, and R is the observation distance from target.

In this paper, we have invented a new strategic technique to extract the reflectivity of each canonical target, which can be used as benchmarks for identifying each target specification and shape. The developed PRMC method is based on the polarimetric properties of the incident and reflected electromagnetic wave relative to the body and orientation of each canonical target. The development of the algorithm concept is based on the simulation and the measurement of the radar cross-section values. First, by choosing the location of the transmitting antenna, the position of the specific target, and the location of the receiving antenna to determine the orientation of the magnetic field that incident on the surface, including the direction of the magnetic field reflected from the object's surface to the receiver antenna. In the next step, the simulation program can perform the processing to resolve the radar cross-section values at each polarization state of each canonical target. Finally, the resulting values may be displayed as a number in matrix form or represented by a colour shade. We then take the values obtained from the measurements and arrange them in matrix form as:

$$\begin{bmatrix} \sigma_{hh,Rx1} \\ \sigma_{vv,Rx1} \\ \sigma_{hh,Rx2} \\ \sigma_{vv,Rx2} \end{bmatrix} \tag{20}$$

to compare with the simulation values. There are several strategies for comparing the results of simulations and measurements depending on the presentation format,

***Table 1**: Simulation and Measurement Parameters.*

Variable	Value
r_1	0.5 m
r_2	0.2 m
r_3	0.1 m
d_1	0.5 m
d_2	0.5 m
d_3	1 m

such as the numeric display and colour gamut. In this paper, we have chosen the correlation coefficients to estimate the potency of the relationship between the relative indications of the two matrix sets. The correlation coefficient is a statistical index used to measure the linear correlation between two vectors. It is a variable that is widely used in the analysis of research results such as in [22] and [23]. The correlation coefficient is defined as the covariance quotient (cov) and standard deviation (std) of two vectors. Suppose there are simulated polarimetric radar cross-section $x = \left[\sigma_{hh,Rx1},\ \sigma_{vv,Rx1}, \sigma_{hh,Rx2}, \sigma_{vv,Rx2}\right]$ and measured samples $y = \left[\sigma_{hh,Rx1},\ \sigma_{vv,Rx1}, \sigma_{hh,Rx2}, \sigma_{vv,Rx2}\right]$, and the sample dimensions are the same; then, the correlation coefficient ρ_{xy} between x and y can be expressed as:

$$\rho_{xy} = \frac{\mathrm{con}\,(\mathrm{x}, \mathrm{y})}{\mathrm{std}\,(\mathrm{x})\,\mathrm{std}\,(\mathrm{y})} \tag{21}$$

where std stands for standard deviation of the variable.

3. EXPERIMENTAL DESCRIPTION

The experiment was conducted in an open area to reduce the reflected wave from the surrounding. Therefore, directional horn antennas with small beamwidth ensure that only the precise signal reflected from the canonical target material was being estimated.

Fig. 3 illustrates the simulation and measurement geometry utilized in this paper. The transmission antenna (Tx) is fixed opposite to the canonical object under test. The receiver antenna (Rx) is positioned on a virtual plane parallel to the wall. Fig. 3(a) displays the transmitting antenna's location relative to the receiving antenna's site, where r_1 stands for the slot in the horizontal axis and r_2 and r_3 present the span in the vertical axis relative to the transmission antenna. As shown in Fig. 3(b), the space between the antenna plane, the wall, and the canonical targets are d_1 and d_2, respectively. The simulation and measurement values used in this paper are r_1 = 0.5 m, r_2 = 0.2 m, r_3 = 0.1 m, d_1 = 0.5 m, d_2 = 0.5 m and d_3 = 1 m, as shown in Tabel 1.

Fig. 4 illustrates the experimental setup and the canonical targets for this investigation. The Keysight signal analyser N9913A module was adapted to generate a continuous signal at the frequency of 1.3 GHz (L-Band), as shown in Fig. 4(a). The RF output is fed via a 1.5 m cable (model: MHD142 RADIALL) to the transmitter (Tx) antenna climbed on a tripod, as shown in Fig. 4(c). The pyramidal horn antennas with a gain of 12 dBi are developed for this employment. They are defined for use with the frequency range from 1.12 GHz to 1.7 GHz based on the standard rectangular waveguide WR-650 configuration and are employed for transmitting and receiving objectives. A similar antenna mounted on a tripod is employed as the receiver (Rx) antenna. It is coupled to RF Input of the Keysight signal analyser N9913A module through a 1.5 m cable, as depicted in Fig. 4(d) and (b), respectively. This experiment investigated three canonical targets: the flat plate (FP) [25 x 25 cm], the vertical dihedral (DV) [25 x 25 cm], and the horizontal trihedral (DH) [25 x 25 cm], as depicted in Fig. 4(e), (f) and (g), respectively. It is divided into three measurements: without obstacles (no wall), brick, and autoclaved aerated concrete walls, as depicted in Fig. 4(h) and (i), respectively.

According to the geometry in Fig. 3, we have defined the incident wave in case of horizontal polarization for the flat plate (FP) as:

$$\overrightarrow{E_h^i} = E_o \hat{x} e^{-j\beta z'} \tag{22}$$

$$\overrightarrow{H_h^i} = \frac{E_o}{\eta}\,(-\hat{y})\, e^{-j\beta z'} \tag{23}$$

and in case of vertical polarization for the flat plate (FP) as:

$$\overrightarrow{E_v^i} = E_o \hat{y} e^{-j\beta z'} \tag{24}$$

$$\overrightarrow{H_v^i} = \frac{E_o}{\eta} \hat{x} e^{-j\beta z'} \tag{25}$$

Due to the geometry of dihedral, we have defined the incident wave in case of horizontal polarization for the vertical dihedral (DV) as:

$$\overrightarrow{E_h^i} = E_o \left(\hat{x}\cos\theta_{\mathrm{i}} + \hat{z}\sin\theta_{\mathrm{i}}\ \right)\ e^{-j\beta\left(x'\sin\theta_{\mathrm{i}} - z'\cos\theta_{\mathrm{i}}\ \right)} \tag{26}$$

$$\overrightarrow{H_h^i} = \frac{E_o}{\eta}\,(-\hat{y})\ e^{-j\beta\left(x'\sin\theta_{\mathrm{i}} - z'\cos\theta_{\mathrm{i}}\ \right)} \tag{27}$$

and in case of vertical polarization for the vertical dihedral (DV) as:

$$\overrightarrow{E_v^i} = E_o \hat{y}\, e^{-j\beta\left(x'\sin\theta_{\mathrm{i}} - z'\cos\theta_{\mathrm{i}}\ \right)} \tag{28}$$

$$\overrightarrow{H_h^i} = \frac{E_o}{\eta}\ \left(\hat{x}\cos\theta_{\mathrm{i}} + \hat{z}\sin\theta_{\mathrm{i}}\ \right)\ e^{-j\beta\left(x'\sin\theta_{\mathrm{i}} - z'\cos\theta_{\mathrm{i}}\ \right)} \tag{29}$$

And, we have defined the incident wave in case of horizontal polarization for the horizontal dihedral (DH) as:

$$\overrightarrow{E_h^i} = E_o \hat{x}\ e^{-j\beta\left(-y'\sin\theta_{\mathrm{i}} - z'\cos\theta_{\mathrm{i}}\ \right)} \tag{30}$$

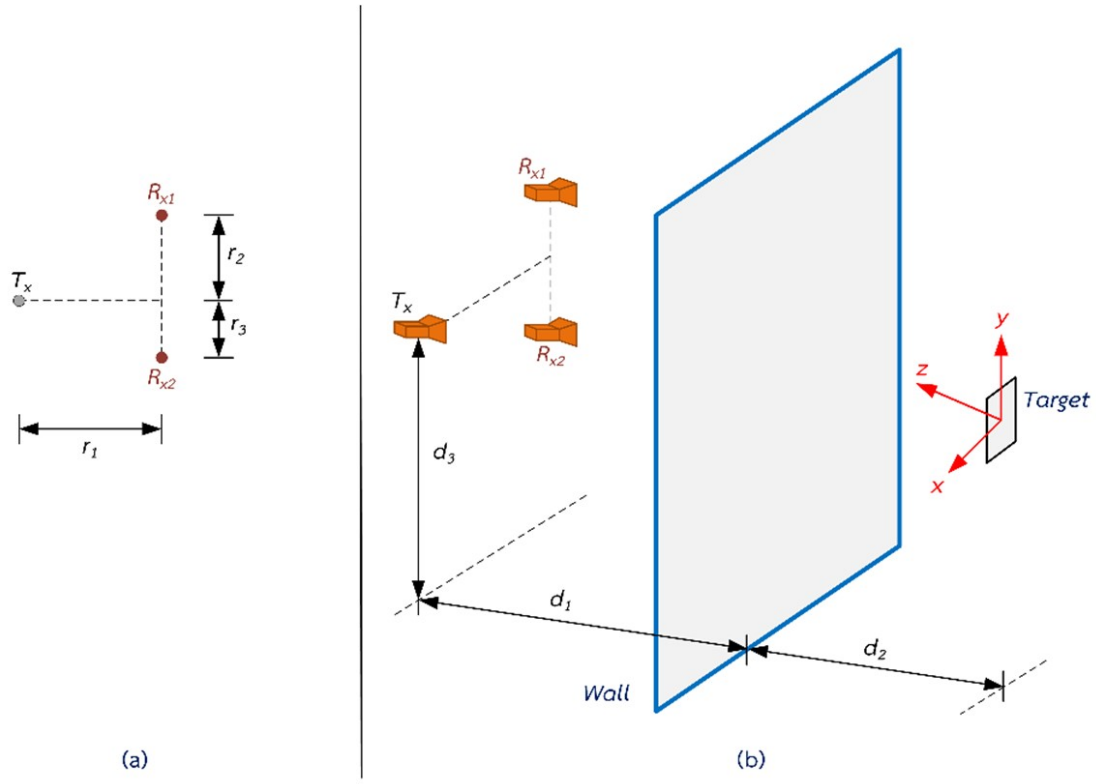

***Fig. 3**: Measurement setup.*

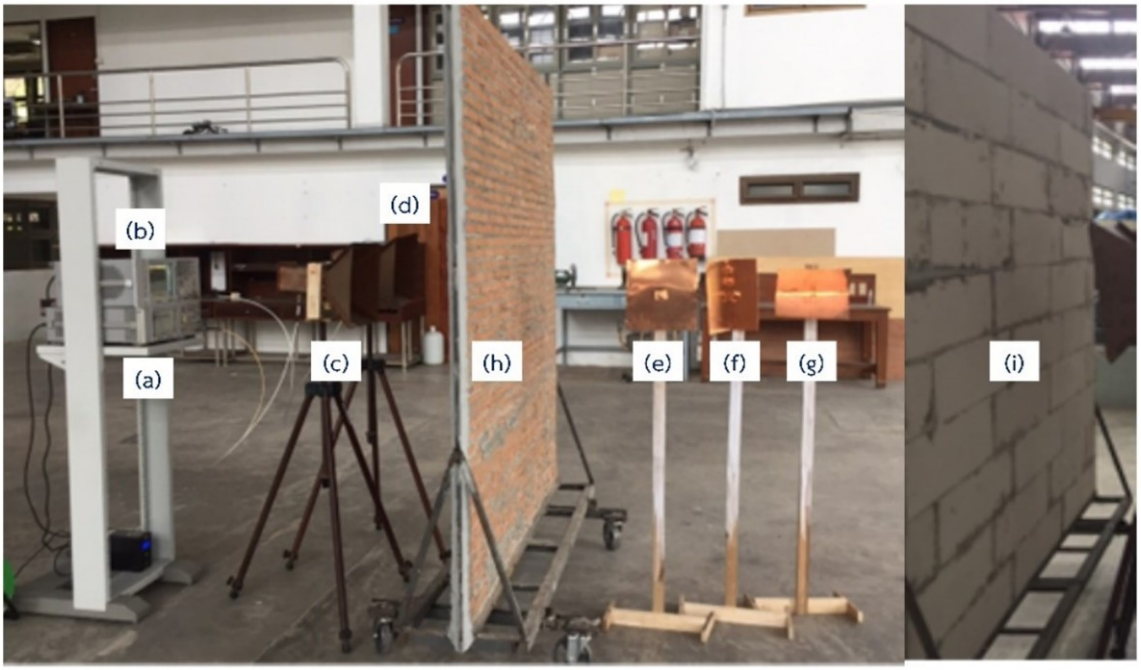

***Fig. 4**: Measurement setup and canonical targets.*

$$\overrightarrow{H_h^i} = \frac{E_o}{\eta}\ \left(-\hat{y}\cos\theta_{\mathrm{i}} + \hat{z}\sin\theta_{\mathrm{i}}\ \right)\ e^{-j\beta\left(-y'\sin\theta_{\mathrm{i}}\ -z'\cos\theta_{\mathrm{i}}\ \right)} \tag{31}$$

and in case of vertical polarization for the horizontal dihedral (DH) as:

$$\overrightarrow{E_h^i} = E_o\left(\hat{y}\cos\theta_{\mathrm{i}} - \hat{z}\sin\theta_{\mathrm{i}}\ \right)\ e^{-j\beta\left(-y'\sin\theta_{\mathrm{i}}\ -z'\cos\theta_{\mathrm{i}}\ \right)} \tag{32}$$

***Table 2**: Simulation and Measurement Results in dB.*

Target	Tx-Rx-Polarization	Simulation	Free Space	Brick-Wall	Concrete-Wall
Flat Plate	$R_{x1,hh}$	-12.57	-12.48	-13.17	-4.93
Flat Plate	$R_{x1,vv}$	-9.37	-10.73	-4.23	-3.15
Flat Plate	$R_{x2,hh}$	-12.07	-13.45	-11.04	-7.06
Flat Plate	$R_{x2,vv}$	-8.36	-12.15	-6.56	-2.31
Vertical Dihedral	$R_{x1,hh}$	-45.00	-9.15	-11.76	-9.15
Vertical Dihedral	$R_{x1,vv}$	-19.77	-8.68	-8.62	-3.18
Vertical Dihedral	$R_{x2,hh}$	-44.98	-10.78	-11.37	-8.25
Vertical Dihedral	$R_{x2,vv}$	-18.96	-5.93	-8.21	-7.21
Horizontal Dihedral	$R_{x1,hh}$	-36.46	-8.39	-10.15	-4.15
Horizontal Dihedral	$R_{x1,vv}$	-38.95	-10.04	-16.07	-11.42
Horizontal Dihedral	$R_{x2,hh}$	-38.24	-7.78	-12.25	-4.04
Horizontal Dihedral	$R_{x2,vv}$	-39.21	-11.79	-15.15	-13.21

***Table 3**: PRMC-Matrix Correlation Coefficient.*

Target	Free Space	Brick-Wall	Concrete-Wall
Flat Plate	0.6195	0.8991	0.8653
Vertical Dihedral	0.7727	0.9940	0.7544
Horizontal Dihedral	0.6748	0.9301	0.8031

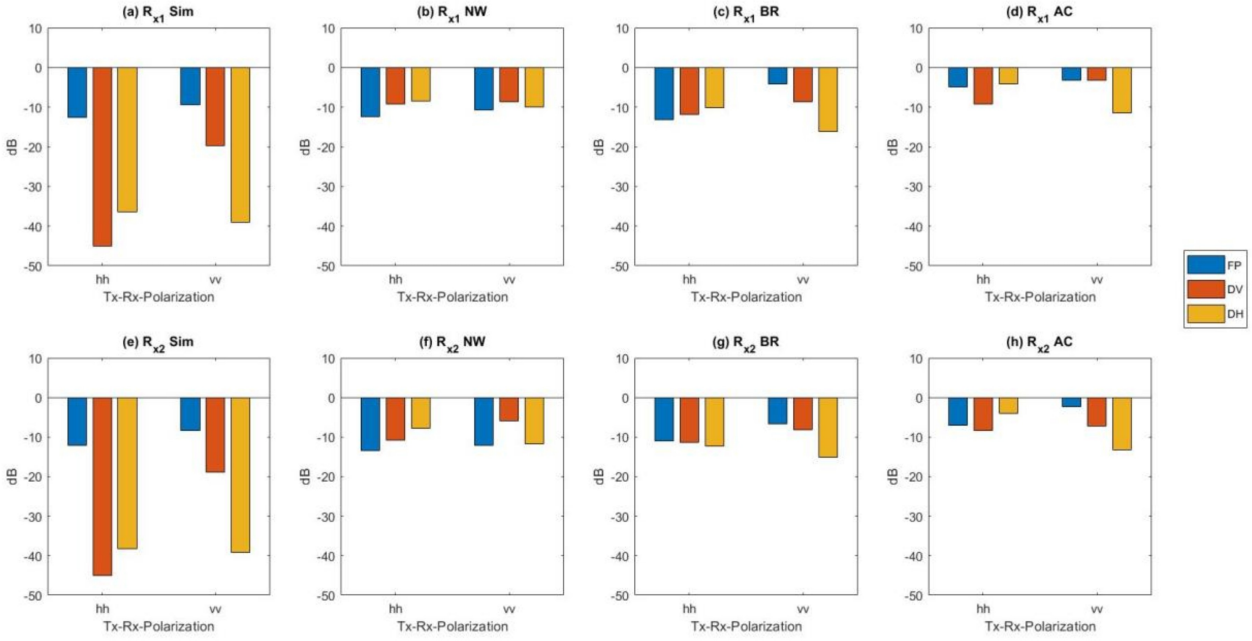

***Fig. 5**: Simulation and measurement results.*

$$\overrightarrow{H_v^i} = \frac{E_o}{\eta}\,\hat{x}\,e^{-j\beta\left(-y'\sin\theta_i\,-z'\cos\theta_i\right)} \tag{33}$$

4. RESULTS AND DISCUSSIONS

4.1 Simulation and Measurement Results

Table 2 shows the results obtained from the simulations and the values obtained from the measurements in dB. The first column is classified according to the specific target type used as a model for processing and measuring actual values. Then, measurements are taken for each target type at two receiving positions (R_{x1}, R_{x2}) using two kinds of polarization (hh, vv). In the 3rd column (Sim.), the values are obtained by simulating the results with the PRMC algorithmic equations. Finally, the 4th, 5th, and 6th columns are the values obtained from the

measurements in no wall conditions (NW), using brick walls (BR), and using autoclaved aerated concrete walls (AC), respectively. Again, we can notice the distinctions due to the position of the receiving antenna and the factors affected by polarization.

Fig. 5 presents the bar graph according to the numerical results in Table 2. In Fig. 5, we aim to compare the PRMC simulation results concerning the measurements. It is demonstrated that the predicted values are compatible with the measured values. Therefore, the distinctions and the correlation between each component can be better illustrated. Fig. 5(a) and 5(e) offer the simulation results of each target type. The measurements in the free space condition are presented in Fig. 5(b) and 5(f). Fig. 5(c) and 5(g) deliver the measurement results using the brick wall. Fig. 5(d) and 5(h) depict the autoclaved aerated concrete wall's measurement results.

4.2 Correlation Coefficient Results

After the PRMC algorithm simulation results and the measured values are obtained, the next step is to estimate the relationship between data sets in the metric format using correlation coefficient values. The correlation coefficient procedures are used to discover how strong an association is between data. The operations return a value between -1 and 1, where: 1 indicates a strong positive relationship, -1 means a robust negative relationship and a result of zero hints at no relationship between two datasets. The following processes are calculated separately for each specific target. First, the base data set or reference data set is obtained from the PRCM simulation, which is then compared with the measured values to determine their correlation.

The results are shown in Table 3. It can be seen that the correlation results obtained are relatively good to an outstanding level both in unobstructed and with wall measurements, mainly by measuring against a brick wall. For example, by measuring flat plate, vertical dihedral, and horizontal dihedral, we get a correlation value of 0.8991, 0.9940, and 0.9301, respectively. An empirical result demonstrates the potential and efficiency of this developed PRMC algorithm by using a few measurements that can be used to determine the geometry or overall shape of a specific target behind an obstacle.

5. CONCLUSIONS

We have ventured into detecting and identifying canonical target shapes hidden by the obstacle. Such a TWRI has excellent applicability in several diverse contexts. To deal with such a problem, we have adopted a PRMC algorithm using a matrix correlation approach based on the polarimetric radar cross-section. We have experimentally validated a PRMC algorithm using 3-D scattering measurement scenarios in semi-controlled conditions. The proposed process takes the values obtained from the simulation results with a computer program as a set or reference value for the values obtained from the measurements, such as the size of the receiver power and the relationship between the antenna position and the shape of each object. Then, measuring instruments and antennas are used to measure the reflection of electromagnetic waves at each point and each polarization. Calculated and measured values are arranged in a matrix to find the value of the relationship with each other. From the experiment, it was found that the matrices would be highly similar. This technique can inspect, measure, and check what shape the objects behind the wall should have. Furthermore, it has been demonstrated that the PRMC can detect and identify the object's shapes in the case of solid scattering objects. In forthcoming expansions, we aspire to address more complex settings with targets regular of practical scenarios. In addition, we are interested in increasing the number of receiving points in another geometry of the antenna array for further complexity of the detecting and identifying procedure.

REFERENCES

[1] K. Sarabandi et al., *Through-the-wall radar imaging*, M.G. Amin, Ed., Boca Raton, FL, USA: CRC Press, 2011.

[2] F. Soldovieri, F. Ahmad and R. Solimene, "Validation of microwave tomographic inverse scattering approach via through-the-wall experiments in semi-controlled conditions," *IEEE Geoscience and Remote Sensing Letters*, vol. 8, no. 1, pp. 123-127, Jan. 2011.

[3] P. C. Chang, R. J. Burkholder, J. L. Volakis, R. J. Marhefka and Y. Bayram, "High-Frequency EM Characterization of Through-Wall Building Imaging," *IEEE Transactions on Geoscience and Remote Sensing*, vol. 47, no. 5, pp. 1375-1387, May 2009.

[4] M. Thiel and K. Sarabandi, "A Hybrid Method for Indoor Wave Propagation Modeling," *IEEE Transactions on Antennas and Propagation*, vol. 56, no. 8, pp. 2703-2709, Aug. 2008.

[5] M. Dehmollaian and K. Sarabandi, "Refocusing Through Building Walls Using Synthetic Aperture Radar," *IEEE Transactions on Geoscience and Remote Sensing*, vol. 46, no. 6, pp. 1589-1599, Jun. 2008.

[6] Y. S. Yoon and M. G. Amin, "Spatial Filtering for Wall-Clutter Mitigation in Through-the-Wall Radar Imaging," *IEEE Transactions on Geoscience and Remote Sensing*, vol. 47, no. 9, pp. 3192-3208, Sep. 2009.

[7] F. Soldovieri and R. Solimene, "Through-wall imaging via a linear inverse scattering algorithm," *IEEE Geoscience and Remote Sensing Letters*, vol. 4, no. 4, pp. 513-517, Oct. 2007.

[8] S. Wu, Y. Xu, J. Chen, S. Meng, G. Fang and H. Yin, "Through-wall shape estimation based on UWB-SP radar," *IEEE Geoscience and Remote Sensing Letters*, vol. 10, no. 5, pp. 1234-1238, Sep. 2013.

[9] F. Soldovieri, R. Solimene and G. Prisco, "A multiarray tomographic approach for through-wall imaging," *IEEE Transactions on Geoscience and*

Remote Sensing, vol. 46, no. 4, pp. 1192-1199, Apr. 2008.

[10] C. Debes, M.G. Amin and A.M. Zoubir, "Target detection in single- and multiple-view through-the-wall radar imaging," *IEEE Transactions on Geoscience and Remote Sensing*, vol. 47, no. 5, pp. 1349-1361, May 2009.

[11] J. Laviada *et al.*, "Broadband synthetic aperture scanning system for three-dimensional through-the-wall inspection," *IEEE Geoscience and Remote Sensing Letters*, vol. 13, no. 1, pp. 97-101, Jan. 2016.

[12] W. Zhang and A. Hoorfar, "Three-dimensional real-time through-the-wall radar imaging with diffraction tomographic algorithm," *IEEE Transactions on Geoscience and Remote Sensing*, vol. 51, no. 7, pp. 4155-4163, Jul. 2013.

[13] A. S. Barzegar, A. Cheldavi, S.H. Sedighy and V. Nayyeri, "3-D Through-the-Wall Radar Imaging Using Compressed Sensing," *IEEE Geoscience and Remote Sensing Letters*, vol. 19, pp. 1-5, 2022.

[14] J. S. Lee and E. Pottier, *Polarimetric radar imaging from basics to applications*, Boca Raton, FL, USA: CRC Press, 2009.

[15] F. Weinmann, "Ray tracing with PO / PTD for RCS modeling of large complex objects," *IEEE Transactions on Antennas and Propagation*, vol. 54, no. 6, pp. 1797-1806, Jun. 2006.

[16] C. Bourlier and P. Pouliguen, "Useful Analytical Formulae for Near-Field Monostatic Radar Cross Section Under the Physical Optics: Far-Field Criterion," *IEEE Transactions on Antennas and Propagation*, vol. 57, no. 1, pp. 205-214, Jan. 2009.

[17] H. Buddendick and T. F. Eibert, "Acceleration of Ray-Based Radar Cross Section Predictions Using Monostatic-Bistatic Equivalence," *IEEE Transactions on Antennas and Propagation*, vol. 58, no. 2, pp. 531-539, Feb. 2010.

[18] C.A. Balanis, *Scattering in Advanced engineering electromagnetics*, New York, USA: John Wiley & Sons, 1989.

[19] Y. Bennani, F. Comblet and A. Khenchaf, "RCS of Complex Targets: Original Representation Validated by Measurements Application to ISAR Imagery," *IEEE Transactions on Geoscience and Remote Sensing*, vol. 50, no. 10, pp. 3882-3891, Oct. 2012.

[20] N. Phruksahiran and M. Chandra, "Polarimetric radar cross section under SAR geometry," *Advances in Radio Science*, vol. 11, pp. 277-282, 2013.

[21] R. Deban, H. Boutayeb, K. Wu and J. Conan, "Deterministic Approach for Spatial Diversity Analysis of Radar Systems Using Near-Field Radar Cross Section of a Metallic Plate," *IEEE Transactions on Antennas and Propagation*, vol. 58, no. 3, pp. 908-916, Mar. 2010.

[22] K. S. Chia and F. W. Hong, "Investigation of Parameters That Affect the Acquired Near Infrared Diffuse Reflected Signals in Non-Destructive Soluble Solids Content Prediction," *Engineering. Journal*, vol. 24, no. 6, pp. 79-90, Nov. 2020.

[23] F. W. Hong, K. S. Chia, and X. Y. Yap, "A Comparison between the Post- and Pre-dispersive Near Infrared Spectroscopy in Non-Destructive Brix Prediction Using Artificial Neural Network," *Engineering. Journal*, vol. 25, no. 10, pp. 39-49, Oct. 2021.

Narathep Phruksahiran received Dipl.-Ing. in Electrical Engineering and Information Technology from the University of the German Federal Armed Forces, Munich, Germany, in 2003 and Dr.-Ing. in Electrical Engineering and Information Technology from the Chemnitz University of Technology, Chemnitz, Germany, in 2013. He is currently an Associate Professor in the Department of Electrical Engineering, at Chulachomklao Royal Military Academy, Nakhon-Nayok, Thailand. His research interests are in spectrum sensing and radio wave propagation.